Chemical and Biological Technologies in Agriculture

RESEARCH

Open Access

Chemical structure elucidation and functional activities comparison of two polysaccharides purified from *Citrus reticulata* Blanco peels

Xiaojun Li[1,2†], Jiang Chen[1†], Yuan Yin[1], Shijun Xiao[1], Rui Zhang[1], Yang Yang[4], Le Li[1], Hairong Xu[1], Xue Zhang[1,2*] and Pei Hu[3*]

Abstract

Background The *Citrus reticulata* Blanco peels have been widely adopted as functional food or nutraceuticals for thousands of years. In our study, two polysaccharides from the *C. reticulata* Blanco peels were obtained and named as CRP-WA and CRP-02A, respectively. After characterization by monosaccharide composition, methylation and NMR, chemical structures of CRP-WA and CRP-02A were elucidated.

Results As a result, CRP-WA with Mw of 32.8 kDa was an arabinogalactan polysaccharide composed of (β1 → 3) (β1 → 3,6)-D-Gal*p*, (β1 → 4)-D-Man*p* and (β1 → 4)-D-Glc*p* units in the backbone. The CRP-02A with Mw of 70.5 kDa was an arabinogalacturonan type pectin formed by (α1 → 4) (α1 → 3,4)-D-Gal*p*A units in the backbone. Moreover, the surface morphologies and rheological properties of CRP-WA and CRP-02A were quite different from each other. Both of these two polysaccharides possessed good antioxidant activities and immunoregulatory effects on RAW 264.7 cells, in which CRP-02A behaved remarkable antioxidant feature, whereas CRP-WA showed relatively high immunoregulatory activity.

Conclusion Our study will provide fundamental information for *C. reticulata* Blanco-based nutritional foods development.

Keywords *Citrus reticulata* Blanco, Arabinogalactan, Arabinogalacturonan, Antioxidant activity, Immunoregulatory effects

†Xiaojun Li and Jiang Chen contributed equally to this work.

*Correspondence:
Xue Zhang
zxue@yzu.edu.cn
Pei Hu
hupei@crjz.com
Full list of author information is available at the end of the article

Graphical Abstract

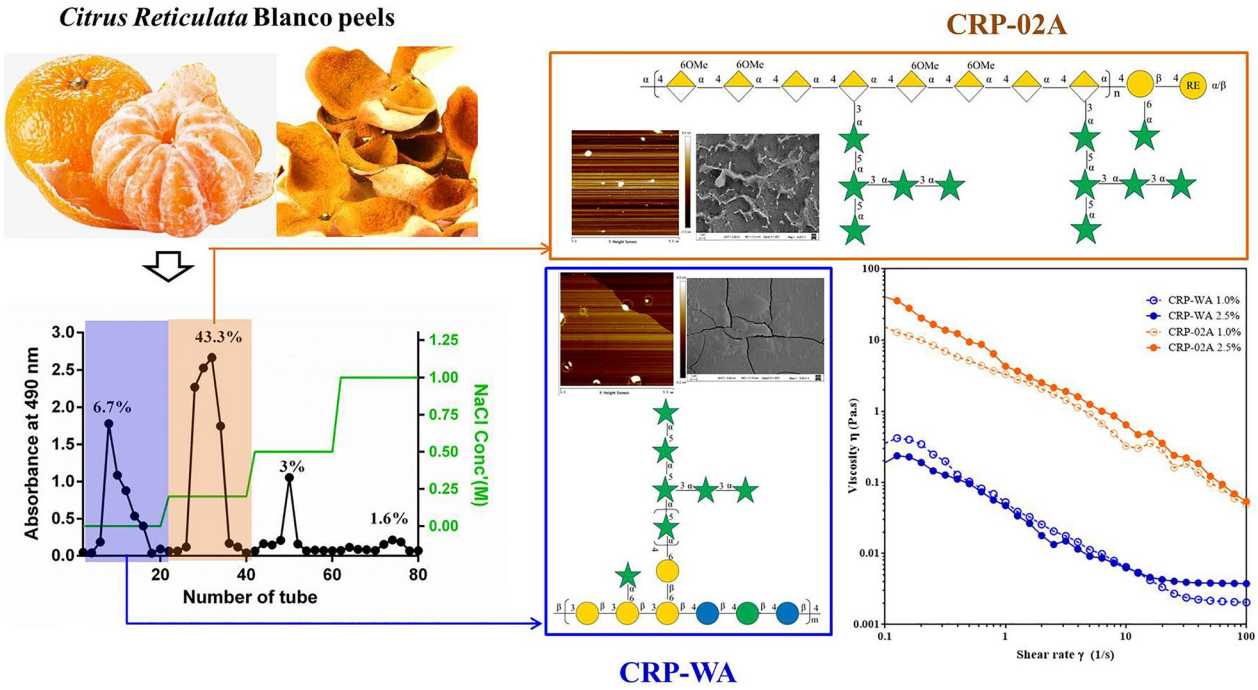

Introduction

There has been enormous interest in the development of pectin as the most valued hydrocolloid in many fields recently [1]. The earliest study on pectin started in 1926 extracted from peels of citrus fruit [1]. *Citrus reticulata* Blanco is evergreen shrub that becomes the most important cash crop of Rutaceae. In China, it is mostly distributed in the south of the Qinling Mountains to the Huaihe River. As for the cultivated varieties of *Citrus reticulata* Blanco, there are 3 varieties [2], including *Citrus reticulata* cv. Dahongpao, *Citrus reticulata* cv. Tangerina as well as *Citrus reticulata* Blanco cv. Chachiensis cultivated in Chongqing, Fujian and Xinhu, respectively, in China. Many parts of *Citrus reticulata* Blanco can be used as medicine, such as immature peels as "Qingpi", mature peels as "Chenpi", seed as "Juhe", leaves as "Juye", and the vascular bundle between mesocarp and endocarp as "Juluo" in Chinese for a long history [3]. The ripe peels of *C. reticulata* Blanco was recorded to resolve phlegm and eliminate dampness, and also was adopted as herbal tea or health-benefit beverage for promoting digestion, treating cough and phlegm, etc. [4].

Current pharmacological researches indicate that the peels of *C. reticulata* Blanco have multiple bioactivities, including regulation of gastrointestinal function, anticancer [5], antioxidant [6] activities, liver protection effect [7] and adjust the blood lipid level [4, 8, 9]. The secondary metabolites from the *C. reticulata* Blanco peels including flavonoids, alkaloids, and essential oils have been thoroughly studied and proven to be the important bioactive components [4]. In addition to these compounds, the primary metabolites including polysaccharides in the peels are also vital bioactive constituents and greatly associated to their health benefits [10]. Importantly, when used as Chinese medicine, the peels of *C. reticulata* Blanco are commonly extracted by boiling water, therefore, the soluble components, particularly polysaccharides accounting for 80% of the total, should be responsible for their bioactivities. Studies on peels of *C. reticulata* Blanco cv. Chachiensis polysaccharides were conducted by [11] and [12]. Further studies are still necessary to dig out more information on the polysaccharides by different isolation and purification methods.

Pectin has been widely explored on its versatile structures and biological activities [13]. Pectin is a kind of Gal*p*A-rich polysaccharide, which has different domains including homogalacturonan, rhamnogalacturonan-I, rhamnogalacturonan-II, xylogalacturonan (XGA) and arabinogalacturonan regions [1]. In which, the arabinogalacturonan domain comprises the Gal*p*A with side

chains of some arabinose and arabinogalactan; whereas, the arabinogalactans (AG) domain has two model types, including linear (β1 → 4)-D-Gal*p* (Type I AG) [14] and (β1 → 3) (β1 → 6)-D-Gal*p* units (Type II AG) [15]. The side chains of AG domain are attached through O-3 of (β1 → 4)-D-Gal*p* (Type I AG) or through different sites of (β1 → 6)-D-Gal*p* units (Type II AG) [15]. The functional attributes of pectin critically rely on its chemical structure, and their diverse structures are critically influenced by the source of the plant as well as by the method of extraction and separation.

However, correlation information is still scarce on the chemical and functional properties of the neutral and pectic polysaccharides isolated from the *C. reticulata* Blanco peels. To gain an additional fundamental understanding of *C. reticulata* Blanco, our study highlighted the different chemical structures of arabinogalactans and arabinogalacturonan type pectin isolated from the peels with the same extraction procedure but different purification methods. The structure-dependent physicochemical, antioxidant and immunoregulatory properties were compared. The potential functional uses of these polysaccharides were unraveled. Our study will provide fundamental information for *C. reticulata* Blanco-based nutritional foods development.

Materials and methods

Materials and reagents

The dried and ripe peels of *Citrus reticulata* Blanco were bought from Bozhou Yinpian Co., Ltd (Anhui, China). DE-52 (BRS008) and Carbohydrate Methylation Kit and were obtained from Yangzhou Borui Saccharide Co., Ltd (Yangzhou, China). 50% NaOH solution for monosaccharide composition study was bought from Alfa Aesar. Dextran standards and monosaccharide standards were bought from Sigma-Aldrich (St. Louis, MO, USA). D_2O and Aceton-D_6 were bought from Aladdin (Shanghai, China). All other reagents used were of analytical grade.

Purification of C. reticulata peel polysaccharides

Extraction of crude CRP

The white piths of the ripe *Citrus reticulata* Blanco peels were removed before polysaccharide extraction. The peels were sliced into pieces and suspended in absolute EtOH overnight at room temperature to remove the pigments. Then, the dried small pieces were suspended in 10 volumes of hot water and boiled for 3 times. After centrifugation at 1000 rpm, the insoluble fractions were discarded, and the supernatant were collected and precipitated by adding EtOH at a final EtOH concentration of 80% and the residues were collected and concentrated. Sequential procedure to remove the proteins and the small molecules were carried out by Sevag procedure (chloroform/n-butanol, v/v = 5:1) and dialysis (MWCO 1000 Da) to remove impurities (Additional file 1: Fig. S1).

Fractionation of crude CRPs

The crude polysaccharides from peels of *Citrus reticulata* Blanco (CRPs) were further purified by two sequential steps. Initially, the crude CRP polysaccharides were purified according to the anion-exchange method. Samples were firstly prepared at 10 mg/mL and subjected onto a DE-52 cellulose anion-exchange column (id. 2.6 × 30 cm) and eluted with water and NaCl solutions. The elutes were separately collected by a fraction collector (Shenzhen Borui Saccharide Co., Ltd, China) and detected by phenol sulfuric assay using microplate reader (Multiskan MK3, ThermoFisher, USA) at 490 nm wavelength.

Then, the collected water and 0.2 M NaCl eluted fractions (CRP-W and CRP-02) were additionally purified according to the size-exclusion chromatography method. The CRP-W and CRP-02 fraction were separated by using a GPC-autopurifier system (BRT-GS, Borui Saccharide, China, www.polyscilife.com). The system was equipped with a RI-502 detector (Shimadzu, Japan) to monitor the eluting fractions and an appropriate gel column (2.6 × 70 cm, Borui saccharide, China) to obtain the homogeneous polysaccharide. The system was eluted by 0.2 M NaCl, and the appropriate fractions were combined by the chromatography results, and concentrated, dialyzed and lyophilized. Two sub-fractions (denominated as CRP-WA and CRP-02A) were finally enriched for further structure, physiochemical properties and bioactivity studies.

Structural characterization of CRPs

Average molecular weight determination by HPGPC

The polysaccharide solution of 3 mg/mL was prepared by dissolving appropriate amount of CRPs sample in 0.05 M NaCl followed by centrifugation. Then, the supernatant was subjected to HPGPC system assembled with a RI detector (RI-10A, Shimadzu, Japan). The column was a tandem BRT 105-104-102 (8*300 mm, Borui Saccharide, China). The previous eluted method was adopted [16]. Commercially available dextran standards (Mw from 5220 to 148,000 Da) were used to calibrate the column. The molecular weights of CRP-WA and CRP-02A were calculated by comparing the retention time to the standards.

Monosaccharide analysis by HPAEC

CRP polysaccharides were firstly hydrolyzed by 3 M TFA at 120 °C. After hydrolyzation for 3 h, the hydrolyzed product was dried under nitrogen air stream, redissolved with water and centrifuged. Then, the hydrolysate and standard monosaccharides were subjected onto

a CarboPac PA-20 column (3 mm × 150 mm, Dionex, Thermo Fisher Scientific). The saccharide constitutes were identified based on their retention time to the standards and data were collected using Chromeleon 7.2 SR4 software.

The total uronic acid content determination

The total uronic acid content (UAC) was determined by the traditional carbazole–H_2SO_4 method with galacturonic acid as a standard according to the previous method with slight modification [17]. Briefly, 0.125% carbazole were prepared by adding 125 mg of carbazole into 100 mL of absolute ethanol. A galacturonic acid standard series (0.03125, 0.0625, 0.125, 0.25, 0.5, 1 mg/mL) were prepared with distilled water. CRP-02A was prepared at 0.5 mg/mL in a test tube. Then, 300 µL of sample or standard solutions were placed in a test tube, 1.5 mL of concentrated sulfuric acid containing 25 mM sodium tetraborate was carefully added. Then, the test tubes were incubated in boiling water bath for 5 min. After cooling to the room temperature, 50 µL of 0.125% carbazole solution was added and boiled for 5 min as well. After cooling to the room temperature, the absorbance of the mixed solution was measured at 540 nm wavelength by a microplate reader (Bio-Tek Synergy2, USA). Based on the absorbance of the standard, the calibration curve was obtained. Then, the UAC of CRP-02A was calculated according to the calibration curve equation of $y = 2.0976 x + 0.3034 (R^2 = 0.9905)$ (Additional file 1: Fig. S2).

FT-IR and UV spectroscopic analysis

FT-IR spectrogram of polysaccharides was recorded by a FT-IR 650 spectrometer (Tianjin Gangdong, China) at 25 °C with spectral range from 400 to 4000 cm^{-1}. In addition, 0.5 mg/mL of the polysaccharides solution was scanned by a microplate reader (Bio-Tek Synergy2, USA) at 25 °C with the wavelength range from 200 to 700 nm.

Methylation analysis

The uronic acid was reduced prior to methylation according to the method described by previously reported protocol [18]. After reduction of the uronic acid, the CRP-WA and CRP-02A were methylated based on the classical method of [19]. A carbohydrate methylation kit (Borui Saccharide Biotech. Co., Ltd, Yangzhou, China) was used according to the manufacturer's instructions and our previous study [16]. The glycosidic linkage identification of CRP-WA and CRP-02A was conducted by analysis of the partially methylated alditol acetates (PMAA) by a QP-2010 GC–MS system (Shimadzu, Japan) according to our previous method [16].

NMR spectroscopic analysis

The dried CRP-WA and CRP-02A were dissolved in D_2O (99.99%D, Alading, China) and lyophilized. The deuterium exchange was repeated in triplicate. Then, the samples were prepared in D_2O at a concentration of 60 mg/mL for NMR analysis by using a Bruker Avance III HD 600 MHz spectrometer. Both of the mono- and bi-dimensional NMR spectra were collected. Chemical shifts of the CRP-WA and CRP-02A were expressed as δ (ppm). The chemical shifts were referenced relative to the DOH signal at δ_H 4.70 ppm. All the NMR spectra were analyzed in MestReNova 14.1.1.

Atomic force microscope (AFM) and SEM analysis

Surface morphology structure of the CRP-WA and CRP-02A were investigated with AFM and SEM. In detailed, the 2D and 3D morphology of the CRP-WA and CRP-02A were characterized by a Bruker Dimension Icon AFM (Dimension ICON, Bruker, USA). Moreover, the microstructure of the polysaccharides surface was examined by using a GeminiSEM 300 (Carl Zeiss, Germany). The freeze-dried CRP-WA and CRP-02A was immobilized on aluminum stubs by double-phase tape and covered with gold for image record. Samples were examined under 5 kV accelerating voltage.

Congo red test and circular dichroism (CD) analysis

The conformation of the CRP-WA and CRP-02A was examined by the Congo red method [20] and CD. Circular dichroism spectroscopy analysis was conducted by using a spectropolarimeter (JASCO J-1500, Tokyo, Japan). Polysaccharides (5 mg) were completely dissolved in deionized water and scanned under 190–260 nm in cells with a 0.1 nm path length. The raw data were graphed by Graphpad V6.01 software.

Rheological tests

The rheological properties of CRP-WA and CRP-02A polysaccharides were tested by a Discovery HR-10 rheometer (TA Instruments, USA) attached with a thermal controller system (TC Peltier) and a 60 mm parallel Peltier. The polysaccharides were prepared at 1% and 2.5% (w/v) in deionized water by dissolving samples for overnight at 25 °C under continuous stirring to ensure complete solubilization. The shear viscosity of all the samples was measured under Flow Sweep mode with shear rate between 0.1 and 100 s^{-1} at 25 ± 1 °C in triplicate.

Antioxidant activities of CRPs

The method reported by [21] was adopted to evaluate the antioxidant capacity of CRPs against the DPPH

free radical. The hydroxyl radical scavenging capacity of CRPs was determined according to the previous method [22]. The method reported by [23] was used to assess the ferric reducing capacity of CRP polysaccharides with slight modification. The method reported by [24] was used to determine the ABTS radical scavenging capacity of CRPs accordingly.

Immunoregulatory activities of CRPs

Cell viability test

RAW 264.7 cells were cultured with DMEM medium supplemented by 10% fetal bovine serum (FBS) and 1% P/S (penicillin and streptomycin) under 37 °C incubator with 5% CO_2 atmosphere. Fifty thousands of RAW 264.7 cells were treated with different concentration of CRP-WA and CRP-02A after attachment on the 96-well plates. After 24 h incubation, 20 μL of MTT (5 mg/mL in PBS) were added and incubated for another 4 h. Then, the supernatant was discarded, and cells were rinsed with PBS (pH7.4) twice and treated with 100 μL of DMSO under dark for 15 min. The absorption was determined by a microplate reader under 570 nm.

Neutral red uptake and NO release assay

The immunoregulatory activities were evaluated by the neutral red uptake and nitrite release of CRPs on RAW 264.7 cells according to the previous methods [25]. The NO contents were determined by Griess agents according to the previous methods [26].

Statistical analysis

Data processing was conducted by Graphpad V6.01 software. Values were expressed as mean ± standard deviation (SD). Data of antioxidant activities and immunoregulatory results were conducted in triplicate. Data of the NMR spectra were processed by MestRenova V6.1.0 software.

Results and discussion

Extraction and purification of polysaccharides from C. reticulata Blanco peels

The yield of the crude polysaccharide (CRP) was around 7% after extraction and precipitation of the *C. reticulata* Blanco peels (Fig. S1). The crude CRP was fractionated by anion-exchange method and named as CRP-W, CRP-02, CRP-05 and CRP-10 according to the eluents used (Fig. 1A, B). The yields of these four fractions were 6.7%, 43.3%, 3.0% and 1.6%, respectively. Then, the major fractions with relative high yield (fraction CRP-W and CRP-02) were further purified with the GPC-autopurifier system. As shown in Fig. 1C, elutes between 80 and 110 min were combined, concentrated, dialyzed, and freeze-dried. This fraction was renamed as CRP-WA with a yield of 18.1%. The main component shown in Fig. 1D from 22 to 42 min fraction was combined, lyophilized. This fraction was named as CRP-02A and the yield was as high as 64.7%.

The Mw and Mn of CRP-WA was estimated to be 32.8 kDa and 22.6 kDa, respectively, and the PDI of CRP-WA was 1.45; for CRP-02A, the Mw and Mn was 70.5 kDa and 49.3 kDa, respectively, and the PDI was 1.43 (Fig. 1G, H),. The low PDI gives the polysaccharide higher solubility [27] and similar molecular weight. These results indicated that the homogenous CRP-WA and CRP-02A were obtained after the sequential processes. Moreover, CPR-02A fraction was relative complicated than CRP-WA due to its relative high molecular weight. These purified polysaccharides will be further used for physical and chemical structure characterization, and biological activities evaluation.

Structural analysis of CRP-WA and CRP-02A

The molar ratios of CRP-WA and CRP-02A were calculated to help reveal important structural information. As shown in Fig. 2A–C, both CRP-WA and CRP-02A were hetero-polysaccharides since the monosaccharide composition is more than one type of monosaccharide. In details, the molar ratio of monosaccharides in CRP-WA was 0.57:0.24:0.07:0.12 for Ara*f*:Gal*p*:Glc*p*:Man*p*, suggesting the neutral polysaccharide of CRP-WA. For the CAP-02A polysaccharide, the monosaccharide Ara*f*, Gal*p* and Gal*p*A was at a molar ratio of 0.34:0.12:0.54, suggesting the pectin nature of the CRP-02A fraction. In addition, the uronic acid content (UAC) of CRP-02A was calculated to be (31.46 ± 0.95)%. Similarly, polysaccharides from the peels of *C. reticulata* Blanco via Chachiensis has been reported to contain pectin polysaccharides [11]. Moreover, the monosaccharide compositions of CRP-WA and CRP-02A differed markedly; residue of Ara*f* is the leading component in CRP-WA fraction, and Gal*p*A is predominate constitute in CRP-02A fraction. Although a minor peak in the position of Gal*p*A showed

(See figure on next page.)

Fig. 1 Fractionation and purification of polysaccharides from peels of *C. reticulata* Blanco. **A** Elution process of crude polysaccharides. **B** Elution curve of polysaccharides from DE-52 column according to the color reaction of phenol sulfuric method. **C** and **D** Elution curves of CRP-W and CRP-02 recorded by GPC Autopurifier system. **E** and **F** Linear of Mw and Mn by HPGPC. **G** HPGPC chromatograms of CRP-W (grey) and CRP-WA (blue). **H** HPGPC chromatograms of CRP-02 (grey) and CRP-02A (orange)

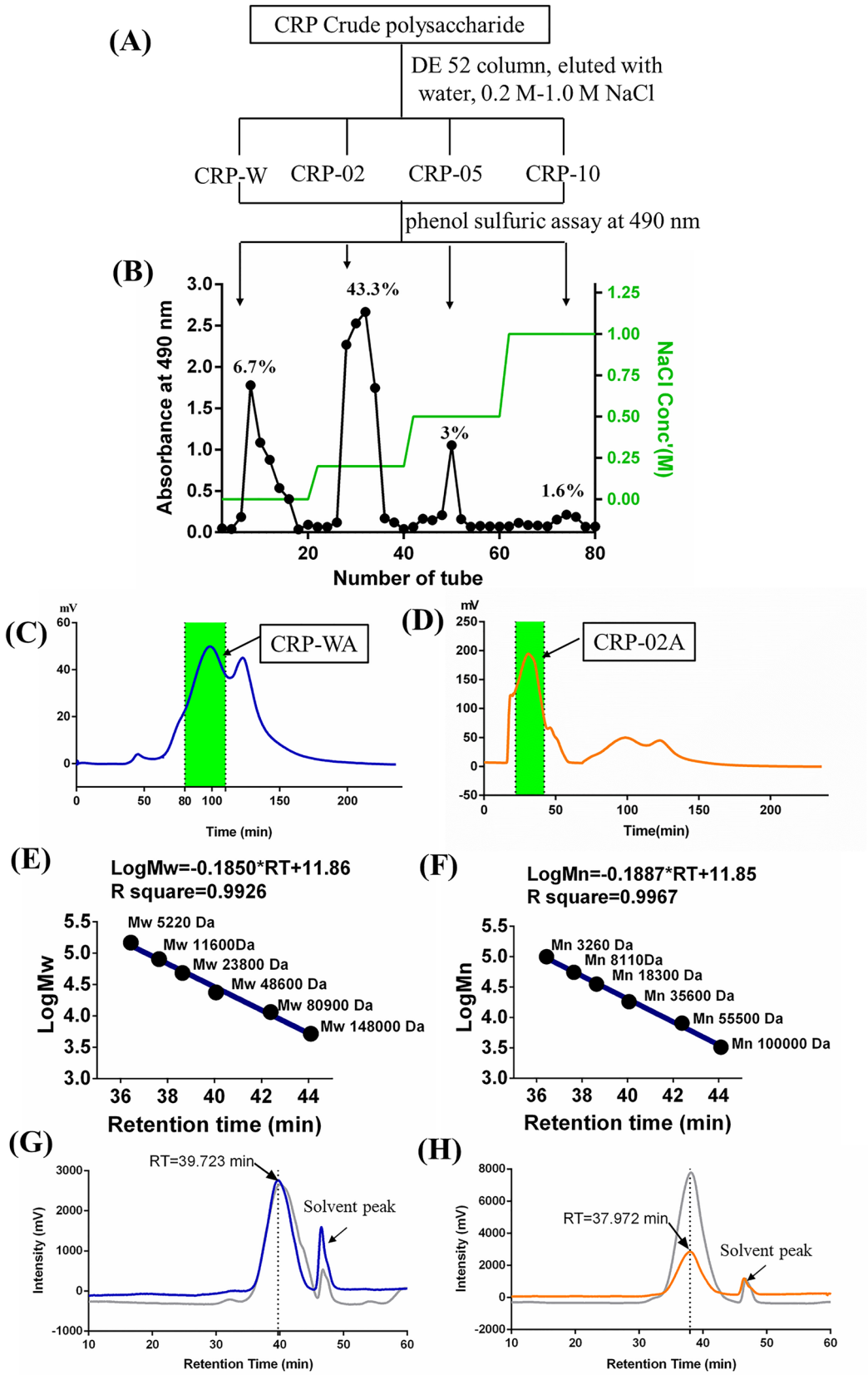

Fig. 1 (See legend on previous page.)

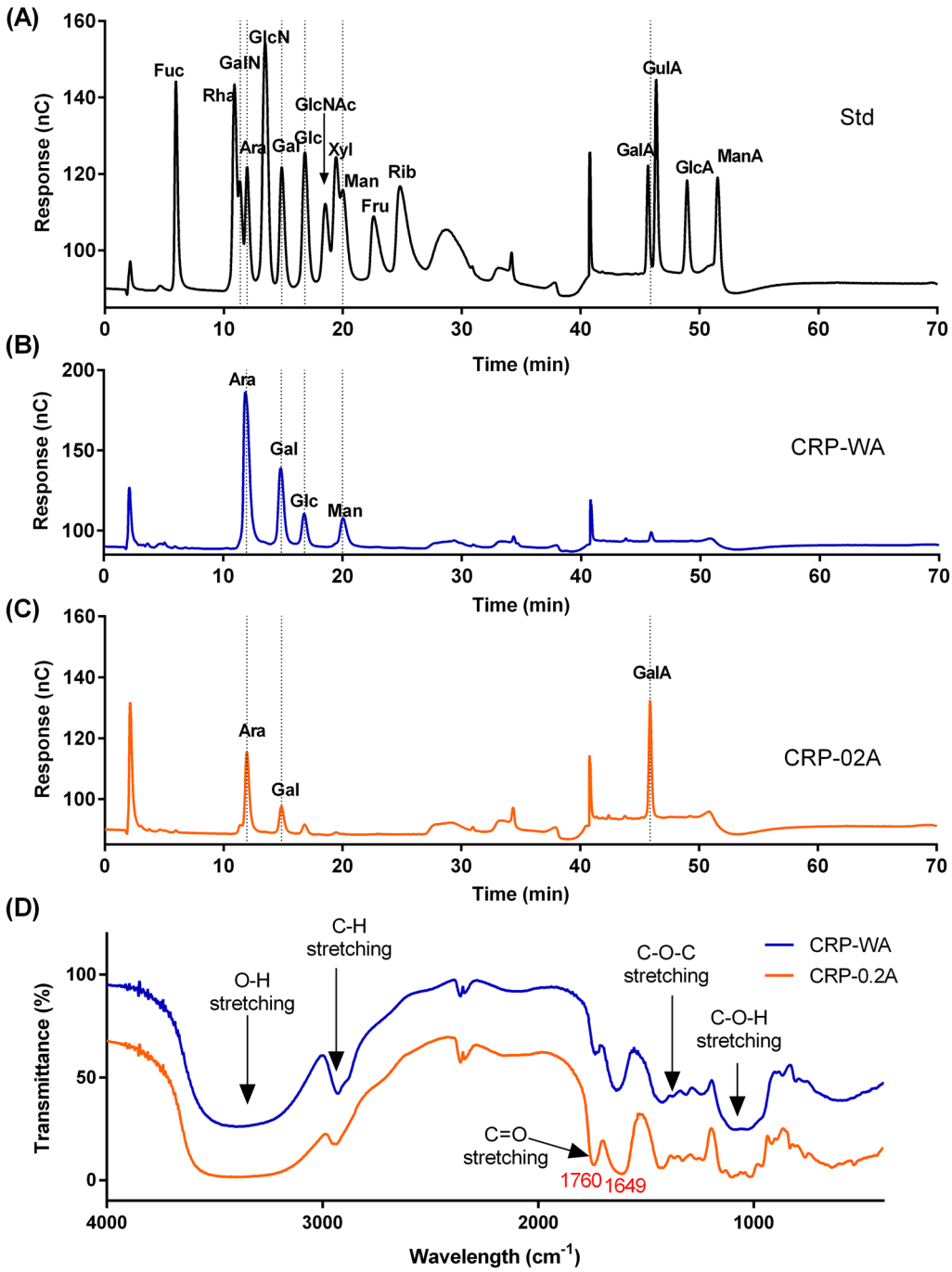

Fig. 2 Monosaccharide composition chromatograms and FT-IR characterization of polysaccharides from peels of *C. reticulata* Blanco. **A** The HPAEC chromatogram of 16 kinds of monosaccharide standards as annotated in the figure. **B** The HPAEC chromatograms of CRP-WA and **C** CRP-02A. **D** FT-IR spectra of CRP-WA and CRP-02A

in the CRP-WA chromatography in Fig. 2B, there are no relative signals of Gal*p*A in the NMR results of CRP-WA, so as the Glc*p* peak in the CRP-02A fraction. These ghost peaks are probably caused by the instrumental or non-instrumental sources [28].

As presented in Fig. 2D, CRP-WA and CRP-02A showed similar absorption bands in FT-IR spectrum except that around 1770-1590 cm^{-1}. Both of CRP-WA and CRP-02A showed a characteristic absorption region around 3180–3570 cm^{-1} of polysaccharide that was

Table 1 Methylation analysis and type of linkage of CRP-WA and CRP-02A

Glycosyl linkage	PMAA derivative	Area percentage (%)*		m/z
		CRP-WA	CRP-02A	
T-Ara*f*	1,4-Di-O-acetyl-2,3,5-tri-O-methyl-arabinitol	46.17	2.55	87, 101, 117, 129, 145, 161, 205
1,3-Ara*f*	1,3,4-Tri-O-acetyl-2,5-di-O-methyl-arabinitol	0.56	n.d	87, 99, 117, 129, 159, 173, 189
1,5-Ara*f*	1,4,5-Tri-O-acetyl-2,3-di-O-methyl-arabinitol	34.50	4.38	87, 101, 117, 129, 161, 173, 189
1,3,5-Ara*f*	1,3,4,5-Tetra-O-acetyl-2-O-methyl-arabinitol	7.90	3.12	85, 99, 117, 127, 141, 159,172, 201, 261
Total Ara		**89.13**[a]	**10.05**	
1,4-Gal*p*	1,4,5-Tri-O-acetyl-2,3,6-tri-O-methyl galactitol	n.d	61.49	87, 101, 117, 129, 161, 173, 233
1,3-Gal*p*	1,3,5-Tri-O-acetyl-2,4,6-tri-O-methyl-galactitol	1.09	n.d	87, 101, 117, 129, 161, 173, 203, 233
1,6-Gal*p*	1,5,6-Tri-O-acetyl-2,3,4-tri-O-methyl-galacitol	0.82	n.d	87, 101, 117, 129, 161, 173, 203, 217, 233
1,3,4-Gal*p*	1,3,4,5-Tetra-O-acetyl-2,6-di-O-methyl galactitol	n.d	15.15	87, 93, 117, 129, 159, 171, 185, 203, 231, 245, 260, 305
1,4,6-Gal*p*	1,4,5,6-Tetra-O-acetyl-2,3,-di-O-methyl galactitol	n.d	10.56	85, 101, 117, 129, 142, 159, 187, 201, 261, 272, 296, 314, 329
1,3,6-Gal*p*	1,3,5,6-Tetra-O-acetyl-2,4-di-O-methyl galactitol	2.22	n.d	87, 101, 117, 129, 159, 173, 189, 233, 273
1,3,4,6,-Gal*p*	1,3,4,5,6-Acetyl-2-O-methyl galactitol	n.d	2.75	77,87, 102,117, 139, 159, 175, 198, 219, 230, 266, 292, 312, 338, 369, 398
Total Gal		**4.13**[b]	**89.95**	
1,4-Man*p*	1,4,5-Tri-O-acetyl-2,3,6-Tri-O-methyl-mannitol	1.00	n.d	87, 99, 117, 129, 143, 161, 173, 203, 233, 281
Total Man		**1.00**[c]		
1,4-Glc*p*	1,4,5-Tri-O-acetyl-2,3,6-tri-O-methyl glucitol	5.74	n.d	87, 99, 117, 129, 161, 173, 189, 233, 253
Total Glc		**5.74**[d]		

* The percentages reported are peak areas from the relative mass detector response (%). n.d = not detected; [a] shows the sum of area percentages of PMAA derivatives from L-arabinofuranosyl residue, [b] shows that from D-galactopyranosyl residue, [c] shows that from D-mannopyranosyl residue and [d] from D-glucopyranosyl residue.

assignable to the stretching vibrations of O–H group. The weak absorption band at 2930–2963 cm^{-1} in CRP-WA and CRP-02A could be attributable to the asymmetric stretching vibration of the C–H group. In addition, two absorption bands around 1455–1463 cm^{-1} and 1000–1158 cm^{-1} were allotted to the stretching vibration of C–O–C and C–O–H group, respectively, suggesting the presence of pyranose ring in CPR-WA and CPR-02A. Importantly, the spectrum of CRP-02A showed a relative strong absorption peak around 1760 cm^{-1} as annotated in Fig. 2D, which was allotted to the asymmetric stretching vibrations of C = O in COO–R group [29], suggesting the methyl-esterified Gal*p*A and much more content of uronic acid and in CRP-02A. These abovementioned results were in correspondence with the saccharide composition results. Moreover, the UV scanning results (Additional file 1: Fig. S3) demonstrated no proteins or other impurity contained in the polysaccharides since no absorption was appeared at 260 nm or 280 nm.

Furthermore, the methylation was conducted to analyze the glycosidic linkage types of CRP-WA and CRP-02A. After comparison of the mass spectra and the retention time to our house methylation library and literature [30], all the peaks in GC chromatogram were identified. The molar ratio of sugar glycosidic linkage types is displayed in Table 1 by calculating their peak areas in GC chromatogram. In CRP-WA, there were nine types of glycosidic linkages and the proportion of the arabinose type glycosyl linkage was 89.13%, whereas in CRP-02A, there were seven types of glycosidic linkages and the proportion of galactose type glycosyl linkage was almost 89.95%. Therefore, it could be concluded that the CRP-WA consisted of a highly branched Ara*f* linkage and CRP-02A was mainly composed of Gal*p* linkage in the backbone.

Importantly, the NMR spectra of CRP-WA and CRP-02A were conducted to confirm and elucidate their structural features (Fig. 3, Fig. 4 and Table 2). For CRP-WA polysaccharide, as shown in Fig. 3A, C, the spectrum exhibited well-resolved signal characteristics of arabinose-type glycosyl linkage. The dominant anomeric resonances in ^{1}H NMR at 5.18 (5.02), 5.08 and 5.04 ppm were identified to T-Ara*f* ($\mathbf{A_t}$, $\mathbf{A_t'}$), (α1 → 5)-L-Ara*f* ($\mathbf{A_5}$)

(See figure on next page.)

Fig. 3 The 1D NMR spectra of the CRP polysaccharides. **A** ^{1}H NMR spectrum of CRP-WA and **B** CRP-02A. **C** ^{13}C NMR spectrum of CRP-WA and **D** CRP-02A. Diagnostic NMR signals are labeled using the following notation: A_t / A_t' = T-Ara*f*, $A_{3,5}$ = (α1 → 3,5)-Ara*f*, A_5 = (α1 → 5)-Ara*f*, A_3 = (α1 → 3)-Ara*f*, $G_{3,6}$ = (β1 → 3,6)-Gal*p*, G_3 = (β1 → 3)-Gal*p*; αG = → 4)- α-D-Gal*p*, eGA_4 = 1,4- Gal*p*A(OMe), CRP = polysaccharides from *C. reticulata* Blanco peels

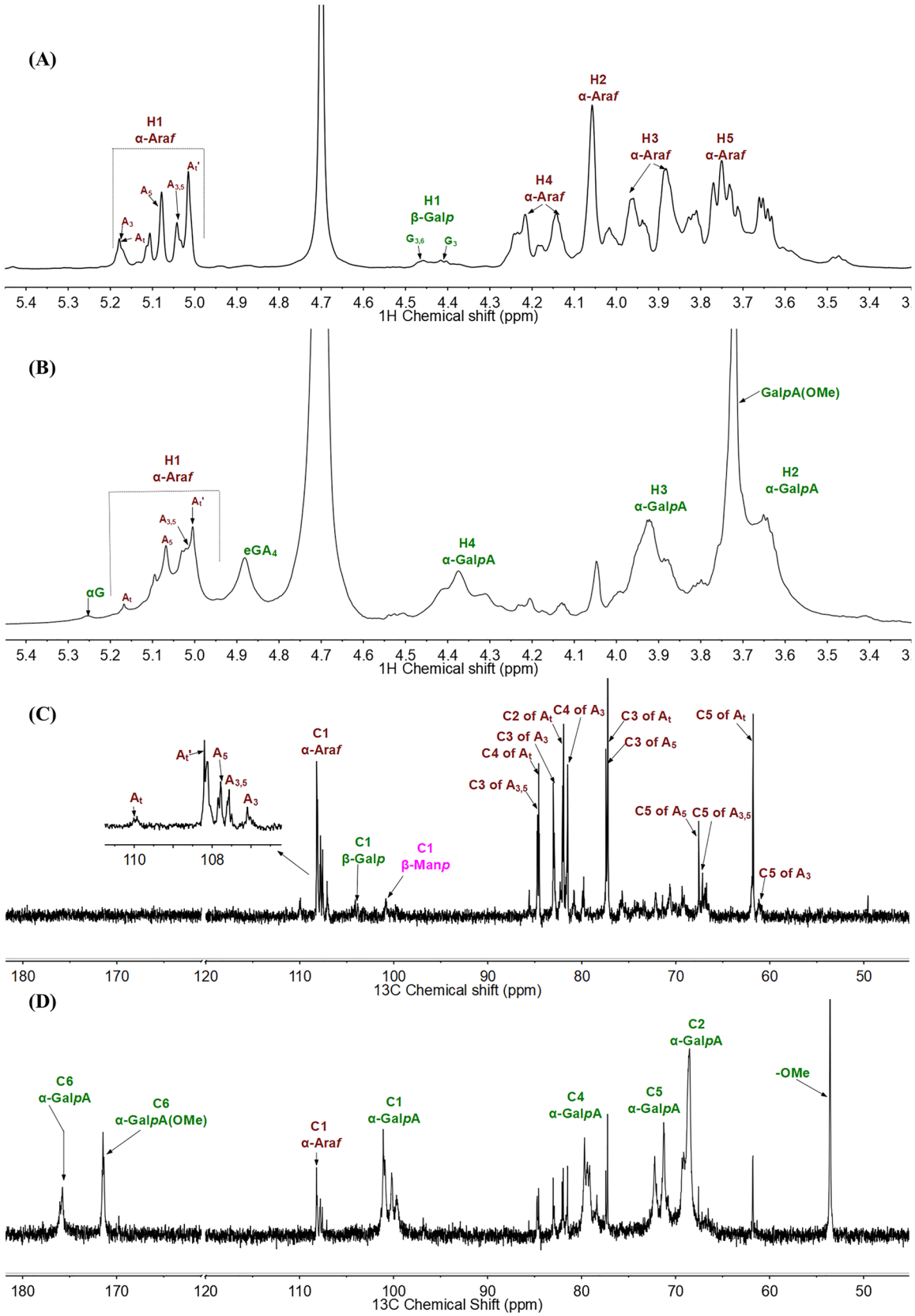

Fig. 3 (See legend on previous page.)

and (α1 → 3,5)-L-Ara*f* (**$A_{3,5}$**), respectively. The increasingly weaker resonances at 4.37, 4.42 and 4.47 ppm were allotted to (β1 → 6)-D-Gal*p* (**G_6**), (β1 → 3)-D-Gal*p* (**G_3**) and (β1 → 3,6)-D-Gal*p* (**$G_{3,6}$**), respectively. The smaller intensity resonances at 4.46 and 4.68 ppm were assigned to (β1 → 4)-D-Glc*p* (**Glc_4**) and (β1 → 4)-D-Man*p* (**M_4**). These assignments were entirely consistent with the literature results [31–34]. Moreover, in the ^{13}C NMR spectrum of CRP-WA, the resonances associated with Ara (110–107 ppm), Gal (~ 104 ppm), Glc (~103 ppm) and Man (~ 100 ppm) were observed [31, 35, 36].

In Fig. 4A, the anomeric region in HSQC spectrum of CRP-WA were enlarged and the distinct cross peaks were observed. On the basis of ^{1}H-^{1}HCOSY and HSQC spectra, signals at δ_H/δ_C at 5.18/110.02, 5.02/108.15 could be assigned to **A_t**/**A_t'**, and 5.18/107.08, 5.08/107.76, 5.04/107.64 can be assigned to **A_3**, **A_5** and **$A_{3,5}$** [37]. Moreover, the chemical shifts at δ_H/δ_C 4.37/104.90, 4.42/104.18 and 4.47/103.84 were assigned to **G_6**, **G_3** and **$G_{3,6}$**. The 4.68/100.84 ppm was assigned to **M_4** and 4.46/103.62 ppm to **Glc_4**. These correlations had been assigned in the HSQC spectra and shown in Fig. 4A. Thus, when we combined the data from ^{1}H and ^{13}C NMR, HSQC and ^{1}H-^{1}HCOSY (Additional file 1: Fig. S4) spectra, comprehensive assignments of all the linkage patterns in CRP-WA have been thoroughly identified and listed in Table 2.

In Fig. 4C, the distinct peaks suggested that H-1 signal of **A_t'** was interrelated to C-5 of **A_5** and C-3 of **A_3** residues. It was also observed that C-1 of **A_5** was correlated to H-5 of **A_5**/**$A_{3,5}$**, and H-6 of **G_6**. Moreover, C-1 of **A_3** was linked to H-3 of **$A_{3,5}$**, and C-1 of **$A_{3,5}$** to H-5 of **A_5**. The C-1 signal of **$G_{3,6}$** was correlated with H-4 of **Glc_4**. In addition, the NOESY spectrum (Fig. 4E) also indicated that the H-1 signal of **$G_{3,6}$** was correlated with its H-3 signal. Other signals also could be observed to show the correlation of **G_3** to **$G_{3,6}$**, and **Glc_4** to **M_4**. The correlations of these residues are also concluded in Table S1. Therefore, the repeating units were deduced and the schematic representation of CRP-WA region structure is shown in Fig. 4G.

For the CRP-02A polysaccharide, the NMR spectra (Fig. 3B, D) revealed intense peaks of methyl-esterified and unesterified Gal*p*A residues according to the literature [38, 39], such as (α1 → 4)-D-Gal*p*A (**GA_4**), (α1 → 4)-D-Gal*p*A(OMe) (**eGA_4**) residues. The existence of **GA_4** in CRP-02A was observed by the signal at δ_C 175.67, whereas the existence of **eGA_4** was ascertained by the resonance at δ_C 171.37, δ_C/δ_H 53.60/3.72 in HSQC spectrum (Fig. 4B2) and δ_C/δ_H 171.37/3.72 in the HMBC spectrum (Additional file 1: Fig. S5) [38, 39].

In detail, in the ^{1}H-NMR spectrum (Fig. 3B), the sharp and strong singlet at δ_H 3.72 was probably caused by the -OCH_3 group of esterified Gal*p*A units. The dominant anomeric resonances in ^{1}H NMR at δ_H 4.88 and 5.03 were probably allotted to anomeric protons of esterified and unesterified Gal*p*A residues, respectively [40]. The anomeric resonances at δ_H 5.17 (5.00), 5.07 and 5.04 were identified to **A_t**/**A_t'**, **A_3** and **$A_{3,5}$** residue. The increasingly weaker resonances at δ_H 5.26 (4.52) and 4.39 were probably assigned to reducing end of α/β-Gal*p* (**αG**, **βG**) and 1,4,6-β-D-Gal*p* (**$G_{4,6}$**). These assignments are entirely consistent to literature results [41–45].

Moreover, as shown in Fig. 3D, the intense peak at 171.37 ppm was probably caused by the carbonyl groups bound to methyl groups (CO-CH_3), and the high-intense signal at 175.67 was produced by all carboxylic acid groups [46]. The sharp and strong singlet at 53.60 ppm resulted from the binding of –CH_3 to -COO groups of Gal*p*A. In the anomeric region of Fig. 3D, four signals at δ_C 107–108 from α-Ara*f* residues were detected, and specifically they belong to **A_t** (at δ_C 107.08 and 108.20), **A_5** (at δ_C 107.99) and **$A_{3,5}$** (at δ_C 107.58), respectively. Three high-intense resonances at δ_C 99–101 from Gal*p*A residues and three low-intense resonances at δ_C 93.15, 96.94 and 104.17 from Gal*p* were also observed detected. It was reported that signals at δ_C 99.79 and δ_C 101.01 ppm were attributed to C-1 of **GA_4** and e**GA** units, respectively [47], and the downfield at 175.67 ppm and upfield at 171.37 ppm were caused by to the C-6 of **GA_4** and methyl-esterified C-6 of e**GA** units [48]. The signals arou nd ~ 100, ~ 68.8, ~ 68.5, ~ 78.7 and ~ 71 ppm were assigned to C-1 to C-5 in skeleton of galacturonic ring, which agree well with previous studies [47, 49].

Cross peaks of these anomeric carbons in CRP-02A to the proton signals are interpreted in Fig. 4B, and the correlation of protons from H-1 to H-6 are annotated in Additional file 1: Fig. S6. Chemical shifts of all carbons and protons were attributed and listed in Table 2. Moreover, distinct cross peaks in Fig. 4D were also observed on

(See figure on next page.)

Fig. 4 The 2D NMR spectra of the CRP polysaccharides. **A** HSQC spectrum of CRP-WA (A1 the anomeric region). **B** HSQC spectrum of CRP-02A (B1 the anomeric region). **C** HMBC spectrum of CRP-WA and **D** CRP-02A. **E** NOESY spectrum of CRP-WA and **F** CRP-02A. **G** Putative structure of CRP-WA and **H** CRP-02A. Diagnostic NMR signals are labeled using the following notation: A_t/A_t' = T-Ara*f*, $A_{3,5}$ = (α1 → 3,5)-Ara*f*, A_5 = (α1 → 5)-Ara*f*, A_3 = (α1 → 3)-Ara*f*, $G_{3,6}$ = (β1 → 3,6)-Gal*p*, $G_{4,6}$ = (β1 → 4,6)-Gal*p*, G_6 = (β1 → 6)-Gal*p*; G_3 = (β1 → 3)-Gal*p*; α/βG = → 4)- α/β-D-Gal*p*; GA_4 = 1,4- Gal*p*A, eGA_4 = 1,4- Gal*p*A(OMe), $GA_{3,4}$ = 1,3,4- Gal*p*A, M_4 = 1,4-Man*p*; CRP = polysaccharides from *C. reticulata* Blanco peels

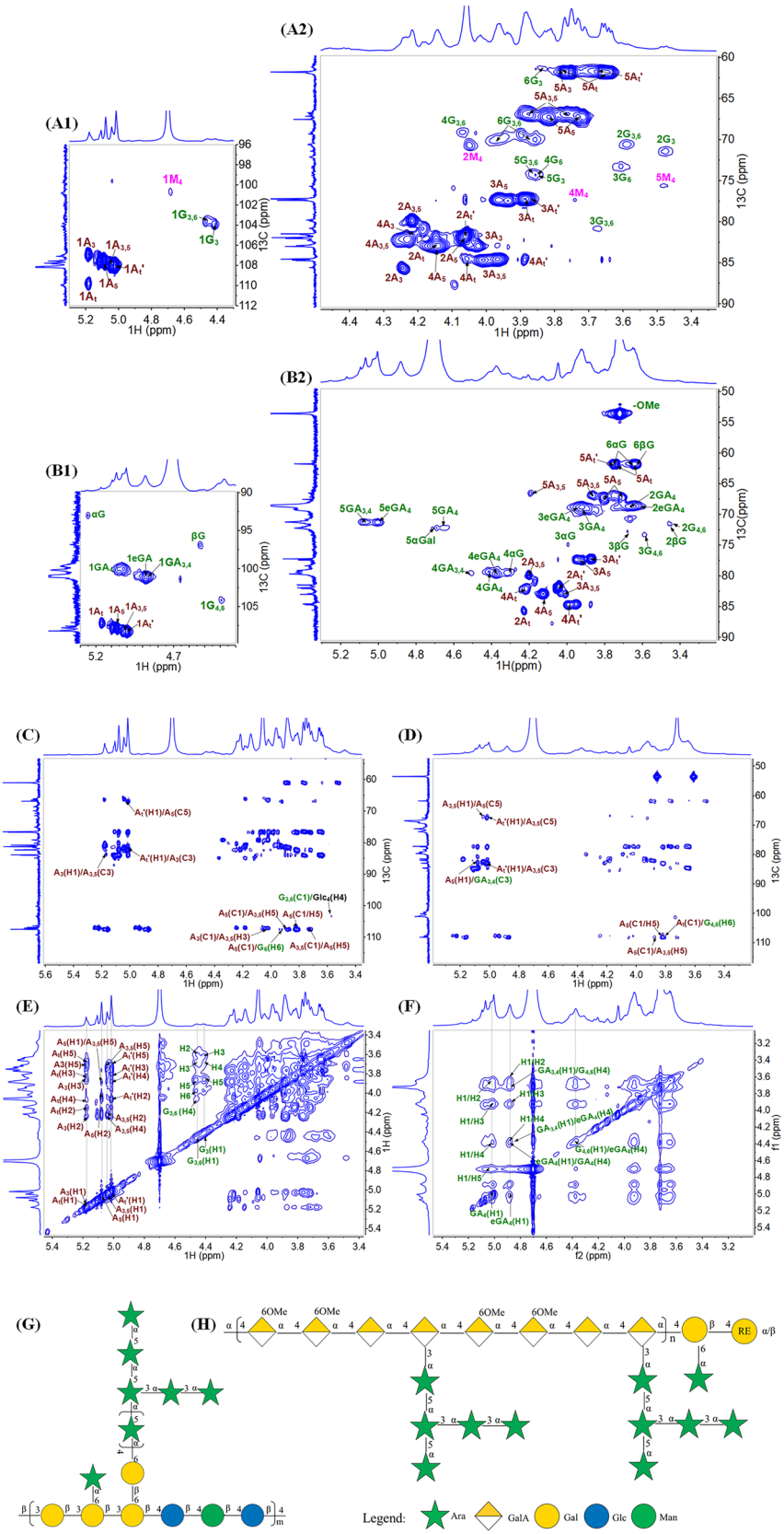

Fig. 4 (See legend on previous page.)

Table 2 Chemical shift assignments of the polysaccharides from peels of *C. reticulata* Blanco using the resonances of -CH_3 groups of acetone

PS	Glycosyl residues	Notation	H-1/C-1	H-2/C-2	H-3/C-3	H-4/C-4	H-5;5′/C-5	H-6;6′/C-6 (O = C-CH3)	O-CH3
CRP-WA	α-L-Ara*f*-(1 →	A_t	5.18/110.02	4.14/82.62	3.87/77.43	4.06/84.57	3.76, 3.64/62.15		
	α-L-Ara*f*-(1 →	A_t'	5.02/108.15	4.06/81.96	3.86/77.80	3.89/84.62	3.69; 3.36/62.33		
	→ 3)-α-L-Ara*f*-(1 →	A_3	5.18/107.08	4.24/85.69	4.03/82.94	4.21/81.49	3.88; 3.78/61.04		
	→ 5)-α-L-Ara*f*-(1 →	A_5	5.08/107.76	4.06/82.25	3.96/77.31	4.14/83.54	3.81; 3.73/67.55		
	→ 3,5)-α-L-Ara*f*-(1 →	$A_{3,5}$	5.04/107.64	4.21/79.90	4.01/84.55	4.25/82.87	3.88; 3.75/66.94		
	→ 6)- β-D-Gal*p*-(1 →	G_6	4.37/104.90	3.44/72.16	3.60/73.47	3.86/74.24	3.88/69.87	3.93; 4.10/70.50	
	→ 3)-β-D-Gal*p*-(1 →	G_3	4.42/104.18	3.48/71.60	3.59/80.73	3.76/72.13	3.85/74.12	3.86/61.77	
	→ 3,6)-β-D-Gal*p*-(1 →	$G_{3,6}$	4.47/103.84	3.60/70.61	3.68/81.50	4.05/69.23	3.87/74.81	3.98; 3.85/70.76	
	→ 4)-β-D-Glc*p*-(1 →	Glc_4	4.46/103.62	3.30/74.17	3.44/76.72	3.58/80.16	3.47/76.69	3.95; 3.79/61.67	
	→ 4)-β-D-Man*p*-(1 →	M_4	4.68/100.84	4.05/70.68	3.73/72.05	3.74/77.23	3.47/75.55	3.82;3.72	
CRP-02A	α-L-Ara*f*-(1 →	A_t	5.17/107.08	4.23/85.81	4.03/82.94	4.21/82.14	3.76; 3.64/61.89		
	α-L-Ara*f*-(1 →	A_t'	5.00/108.20	4.05/82.7	3.87/77.59	3.98/84.94	3.75; 3.65/61.82		
	→ 5)-α-L-Ara*f*-(1 →	A_5	5.07/107.99	4.07/81.22	3.93/77.31	4.13/83.11	3.81; 3.79/67.25		
	→ 3,5)-α-L-Ara*f*-(1 →	$A_{3,5}$	5.04/107.58	4.21/80.48	4.00/82.97	4.25/81.32	4.19;3.87/66.98		
	→ 4)-α-D-Gal*p*	αG	5.25/93.15	3.74/69.6	3.99/75.07	4.34/79.12	4.72/72.7	3.73; 3.65/61.43	
	→ 4)-α-D- Gal*p*A-(1 →	GA_4	5.03/99.79	3.68/68.8	3.93/68.67	4.37/78.76	4.68/72.29	175.67	
	→ 4)-α-D-Gal*p*A(OMe)-(1 →	eGA_4	4.88/101.01	3.64/68.8	3.93/68.8	4.39/78.65	5.05/71.26	171.37	3.72/53.60
	→ 3,4)-α-D- Gal*p*A-(1 →	$GA_{3,4}$	4.87/101.27	4.17/72.7	4.09/82.55	4.51/79.76	5.07/71.83	175.67	
	→ 4)-β-D-Gal*p*	βG	4.52/96.94	3.45/71.81	3.68/73.03	4.27/79.19	4.66/72.75	3.75; 3.63/61.76	
	→ 4,6)-β-D-Gal*p*-(1 →	$G_{4,6}$	4.39/104.17	3.46/71.64	3.64/73.30	3.71/83.02	3.83/74.61	3.93;3.81/68.72	

H-1 of $\mathbf{A_t'}$ to C-5 of $\mathbf{A_5}$, H-1 of $\mathbf{A_t'}$ to C-3 of $\mathbf{A_{3,5}}$, H-1 of $\mathbf{A_{3,5}}$ to C-5 of $\mathbf{A_5}$, H-1 of $\mathbf{A_5}$ to C-3 of (α1 → 3,4)-D-Gal*p*A ($\mathbf{GA_{3,4}}$), suggesting the side chains of CRP-02A were linked to the main chain via O-3 position of $\mathbf{GA_{3,4}}$ residue. In addition, inter-residue correlation peaks were clearly observed on δ_H 4.88 (H-1 of $\mathbf{eGA_4}$) to δ_H 4.39 (H-4 of $\mathbf{eGA_4}$) and δ_H 4.37 (H-4 of $\mathbf{GA_4}$), δ_H 5.03 (H-1 of $\mathbf{GA_4}$) to δ_H 4.51 (H-4 of $\mathbf{GA_{3,4}}$), δ_H 4.87 (H-1 of $\mathbf{GA_{3,4}}$) to δ_H 4.39 (H-4 of $\mathbf{eGA_4}$) in the ^1H-^1H NOESY spectrum (Fig. 4F) confirmed the occurrence repeating the tetrasaccharide units [→4)-α-D-Gal*p*A(OMe)-(1 → 4)-α-D-Gal*p*A(OMe)-(1 → 4)-α-D-Gal*p*A-(1 → 3,4)-α-D-Gal*p*A-(1 →] in CRP-02A. A schematic representation of CRP-02A polysaccharide structure is presented in Fig. 4H.

In summary, the structural features of CRP-WA and CRP-02A could be concluded from the abovementioned NMR results as follows: (i) CRP-WA is AG-II type polysaccharide; (ii) the backbone of CRP-WA comprises (β1 → 3)(β1 → 3,6)-D-Gal*p*, (β1 → 4)-D-Glc*p* and (β1 → 4)-D-Man*p* units; (iii) the following residues were identified in the side chain of CRP-WA: (α1 → 5) (α1 → 3,5) (α1 → 3)-L-Ara*f* units; (iv) CRP-02A is a member of pectic arabinogalacturonan family; (v) the backbone of CRP-02A contains (α1 → 4)(α1 → 3,4)-D-Gal*p*A and (α1 → 4,6)-D-Gal*p* units; (vi) the side chain of CRP-02A branched at O-3 of (α1 → 3,4)-D-Gal*p*A by (α1 → 5) (α1 → 3,5)-L-Ara*f* units. Moreover, this proposed structure AG-II of CRP-WA was not the same as the classical AG-II model, which assumes that only (β1 → 3)-D-Gal*p* presented in the main chain with (β1 → 6)-D-Gal*p* in the side chains [36].

Micromorphology analysis of CRP polysaccharides

As shown in Fig. 5A, B, the CRP-WA and CRP-02A contained spherical structures in different sizes, indicating the presence of aggregation or intertwined polysaccharides molecules. The height of polysaccharide with a single chain structure was reported to be in the range of 0.1–1.0 nm [50]. However, the height of CRP-WA was between − 5.2 and 6.8 nm, and that of CRP-02A was between − 7.3 and 8.0 nm. The relatively high height of the CRP-WA and CRP-02A indicated the aggregation probably formed by the van der Waals forces between the main chain and the highly branched Ara*f* in CRP-WA

and CRP-02A. In addition, CRP-WA exhibited a tight and dense laminar structure similar to cracked pavement. CRP-02A showed a relative looser "rippled" lamellar shape (Fig. 5C), which agreed with the previous pectin morphology [51]. The sugar content analysis showed that CRP-WA had the large amount of neutral Ara*f*, and the large amount of Ara*f* located on the side chains. However, CRP-02A displayed a loose lamellar morphology, which could be probably induced by the overall negative charges that hindered the aggregation of pectin chains.

Conformation properties of CRP polysaccharides

Since conformations of polysaccharide are closely related to their functional properties, we characterized the conformation difference of polysaccharide molecules by CD spectra (Fig. 5D) and Congo red test (Fig. 5E). The CD is implemented to study the conformational changes of the polysaccharide, which is a popular method to identify the triple-helix shape in solid-state or in solutions. CD spectrum of CRP-WA and CRP-02A exhibited positive cotton effect at ~ 206 nm. The result of CRP-WA and CRP-02A were consistent with red shift phenomenon when compared to the control of Congo red at the same NaOH concentration. These results indicated the existence of triple helical conformation of CRP-WA and CRP-02A, which agree with the previous studies [20].

Rheological properties of CRP polysaccharides

The flow behavior characterization of CRP-WA and CRP-02A were evaluated and compared. The viscosity of CRP-WA and CRP-02A showed gradually decreased when the shear rate increased, indicating a shear-thinning behavior of the CRPs polysaccharide (Fig. 5F). Such pseudo-plastic property is probably caused by the disentanglement of polysaccharides along the shear flow direction under the low shear force, thus causing a gradual reduction in the viscosity, which agrees with the previous data [52]. Besides, the steady-state viscosity for all CRP-02A concentrations was higher than that of CPR-WA by at least ten times, which is probably caused by the high molecular weight (Mw 70.5 kDa of CRP-02A and Mw 32.8 kDa for CRP-WA) and the chemical content of CRP-02A.

Antioxidant activities evaluation

As shown in Fig. 6A, CRP-WA and CRP-02A were capable to scavenge DPPH radicals within the tested range. The DPPH scavenging ability of CRP-02A reached (68.3 ± 3.7)% as more than twice of CRP-WA (30.9 ± 1.9)% at the tested polysaccharide concentration of 2 mg/mL. Moreover, CRP-WA and CRP-02A showed relatively high hydroxyl radical scavenging activity in the tested polysaccharide concentrations (Fig. 6B). Furthermore, both of these two polysaccharides showed strong scavenging capacity of ABTS free radical in a concentration-dependent manner (Fig. 6C), whereas it reached a maximum value of (83.1 ± 1.9)% for CRP-WA and (98.4 ± 0.8)% for CRP-02A, respectively, at 2 mg/mL of polysaccharide solution. Generally, the stronger reduction power indicated the higher antioxidant ability, and the reduction power of CRP-WA and CRP-02A displayed an increasing trend with the polysaccharide concentration increased (Fig. 6D). The reducing abilities of CRP-WA and CRP-02A were (9.9 ± 1.9)% and (32.9 ± 1.5)%, respectively, at 2.0 mg/mL polysaccharide, representing better reducing power of CRP-02A than that of CRP-WA. More importantly, we reduced the uronic acid groups in CRP-02A to further verify whether the uronic acid groups play an important role in the antioxidant activities. The antioxidant activities of reduced CRP-02A were relatively poor when compared to than that of native CRP-02A in DPPH radical scavenging, ABTS radical scavenging and ferric reduction (Additional file 1: Fig. S7), suggesting the potential contribution of uronic acid groups from CRP-02A to the antioxidant activities.

Immunoregulatory activities evaluation

As shown in Fig. 7A, cell viability of RAW 264.7 cells was increased after both CRP-WA and CRP-02A treatment at the concentration from 1.25 to 40 μg/mL, indicating the non-toxicity of CRP-WA and CRP-02A within this concentration range but growth promotion effects of RAW 264.7 cells. When the polysaccharide concentration reached to 80 μg/mL, cells were slightly inhibited when compared to the control group with cell culture medium treatment. When macrophages are activated, their phagocytosis ability could be enhanced [53]. Therefore, the neutral red uptake ability of RAW 264.7 cells after polysaccharide treatment was evaluated in this study. As a result, the phagocytosis index of CRP-WA showed an increased trend at the concentration from 10 to 80 μg/mL but did not reach the significance when compared to the blank control group. The phagocytic ability of RAW

(See figure on next page.)

Fig. 5 The morphological, conformational and flow behaviors of polysaccharides from *C. reticulata* Blanco peels. **A** The 2D images of CRP-WA and CRP-02A. **B** The 3D images of CRP-WA and CRP-02A. **C** The SEM images of CRP-WA and CPR-02A at magnification of 5000×. **D** The CD spectra; **E** the Congo red results of CRP-WA and CRP-02A at 0.1–0.5 M NaOH concentration. **F** Rheological observation of steady-state viscosity of CRP-WA and CPR-02A at concentration of 1.0% and 2.5% (w/v)

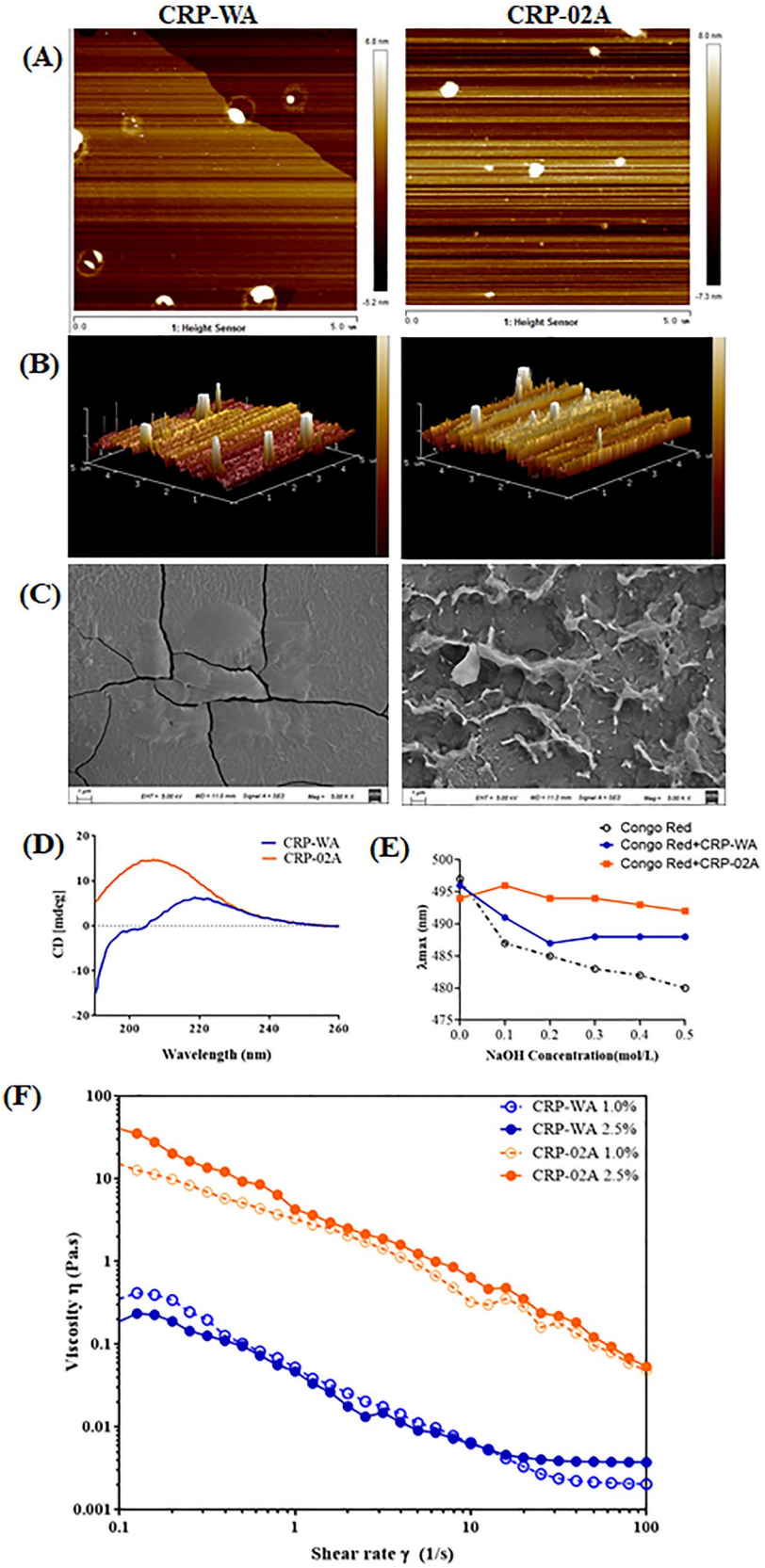

Fig. 5 (See legend on previous page.)

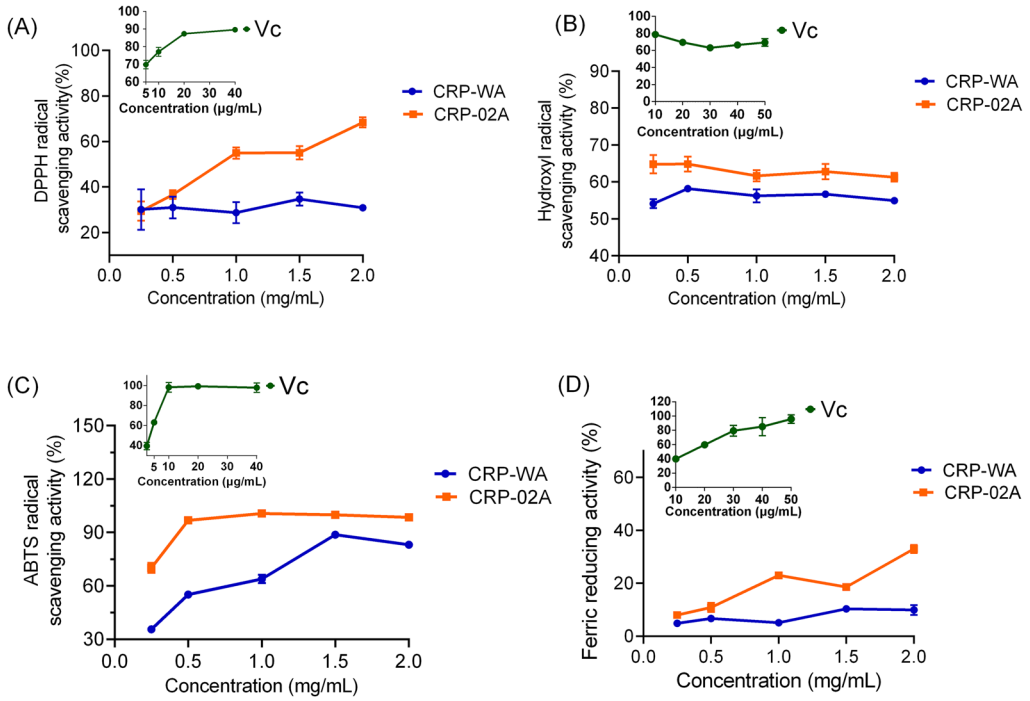

Fig. 6 Antioxidant activities of CRP-WA and CRP-02A. The radical scavenging capacity of **A** DPPH, **B** hydroxyl radical, **C** ABTS and the ferric reducing activity **D**

264.7 cells induced by the CRP-02A showed a poor effect (Fig. 7B). The release of NO is reported to be a fundamental signaling compound secreted by the activated RAW 264.7 cells [54]. In our present study, the NO release was enhanced when cells treated with CPR-WA compared to the control group (Fig. 7C). In some ways, CRP-WA had immunoregulatory effects on RAW 264.7 cells.

Consequently, polysaccharides from peels of *Citrus R.* Blanco showed significant antioxidant activities and immunoregulatory effects to some extent on RAW 264.7 cells. Further, CRP-02A displayed stronger antioxidant capacity than that of CRP-WA. These antioxidant differences of CRP-WA and CRP-02A might be attributed to the result of compositional differences in structural polysaccharides, the branched degree. The molecular weight seems to be of little importance for activity. CRP-02A was an arabinogalacturonan type pectin structure with a relative high molecular weight, whereas CRP-WA was an arabinogalactan structure with a relative low molecular weight. The high content of uronic acids in CRP-02A could donate plenty of protons to reduce the DPPH, hydroxyl radical, ABTS radical and reduction of Fe^{3+}.

Conclusions

In this study, two water-soluble polysaccharides purified from the peels of *C. reticulata* Blanco by fractionation of the crude polysaccharide into neutral and pectic fraction. The structural characteristics of the homogenous CRP-WA and CRP-02A were explored in-depth. The results from molecular weight and monosaccharide composition analysis showed that CRP-WA with Mw of 32.8 kDa had Ara*f* as the major component of the polysaccharide, while CRP-02A with Mw as high as 70.5 kDa had the Gal*p*A as the main composition. Methylation and NMR results further verified the chemical structure and confirmed that CRP-WA was a neutral polysaccharide of AG-II which consisted mainly of a (β1 → 3)-β-Gal*p* in the backbone, with Ara*f* substituents at O-6 of (β1 → 3,6)-D-Gal*p* residues, whereas CRP-02A was a pectic polysaccharide with the backbone comprising (α1 → 4)-D-Gal*p*A residues that decorated methyl ester groups at the galacturonan backbone. Moreover, CRP-02A showed a higher viscosity but looser surface structure than that of CRP-WA, which was probably due to the chemical structure of CRP-WA with longer and larger arabinose branches than that of CRP-02A. The antioxidant results demonstrated that both of the two soluble polysaccharides possessed potential

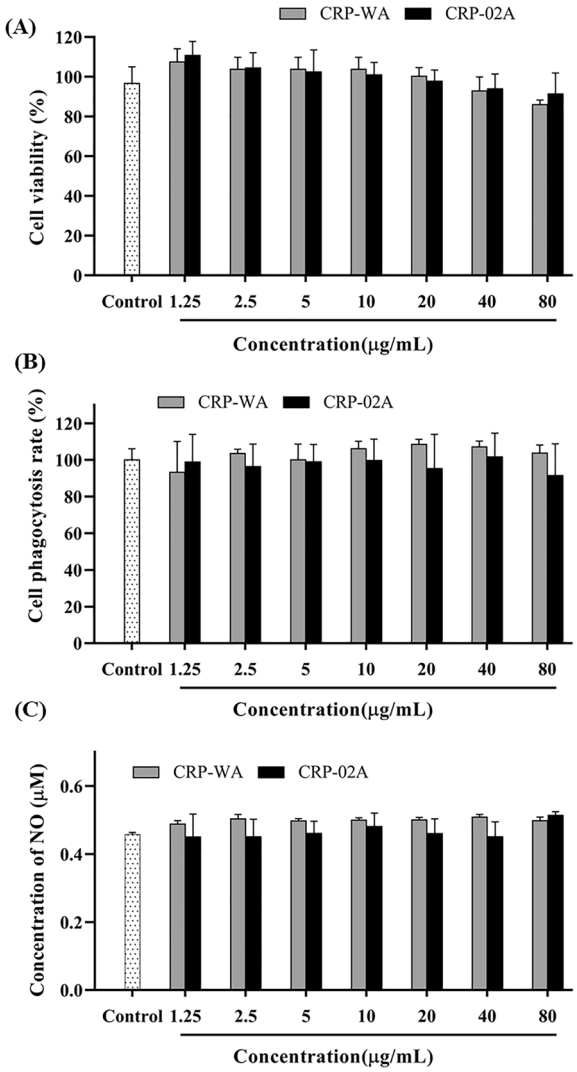

Fig. 7 Immunoregulatory effects of CRP-WA and CRP-02A evaluated by RAW 264.7 cells. **A** MTT results of CRP-WA and CRP-02A on RAW 264.7 cells. **B** Phagocytosis index of CRP-WA and CPR-02A on RAW 264.7 cells by neutral red uptake. **C** NO release induced by CRP-WA and CRP-02A on RAW 264.7 cells by Griess agents method

antioxidant effects, in which CRP-02A was more pronounced. All these results helped gain a more fundamental understanding of *C. reticulata* Blanco, and provided a preliminary exploration of polysaccharides from peels of *C. reticulata* Blanco as potential antioxidants.

Supplementary Information

The online version contains supplementary material available at https://doi.org/10.1186/s40538-024-00556-2.

Additional file 1: Figure S1. Scheme of extraction of crude polysaccharides from peels of *Citrus reticulata* Blanco. **Figure S2** The standard curve of standard galacturonic acid from 0.03125-1.0 mg/mL. **Figure S3.** UV scanning of polysaccharides from peels of *Citrus reticulata* Blanco. **Figure S4.** HHCOSY NMR spectrum at of CRP-WA. **Figure S5.** The whole HMBC spectrum of CRP-02A. **Figure S6.** HHCOSY NMR spectrum at of CRP-02A. **Figure S7.** Antioxidant activities of CRP-02A before and after uronic acid reduction (Reduced CRP-02A) in DPPH radical scavenging (A), hydroxyl radical scavenging (B), ABTS radical scavenging (C) and ferric reducing activity (D). **Table S1**. The correlations between the glycosidic residues in CRP-WA and CRP-02A.

Acknowledgements

This study was financially supported by the National Natural Science Foundation of China (No. 82304133), the Natural Science Foundation of Jiangsu Province (Nos. BK20210818, BK20230590), the Natural Science Foundation of the Jiangsu Higher Education Institutions of China (No. 21KJB360023 and No. 22KJB310025), the fellowship of China Postdoctoral Science Foundation (No. 2020M671636), and the Administration of traditional Chinese medicine of Jiangsu Province (No. QN202227) and the Postgraduate Research & Practice Innovation Program of Jiangsu Province (No. SJCX23_2044).

Author contributions

XJL: Conceptualization, Methodology, Supervision, Data Curation, Funding acquisition. JC: Investigation, Data Curation, Validation, Visualization. YY: Visualization, Investigation, Validation. SJX and RZ: Validation: LL: Resources and Investigation; YY: Writing- Review & Editing and Funding acquisition; HRX: Writing- Review & Editing; XZ: Supervision, Visualization, Writing- Reviewing and Editing, Formal analysis, Funding acquisition; PH: Software, Validation, Resources, Investigation, Formal analysis.

Availability of data and materials

No datasets were generated or analysed during the current study.

Declarations

Competing interests

The authors declare no competing interests.

Author details

[1]Institute of Translational Medicine, Medical College, Yangzhou University, Yangzhou 225001, China. [2]Jiangsu Key Laboratory of Integrated Traditional Chinese and Western Medicine for Prevention and Treatment of Senile Diseases, Yangzhou University, Yangzhou 225001, China. [3]Jiangzhong Pharmaceutical Co., Ltd., No.1899 Meiling Road, Nanchang 330103, China. [4]Guangling College, Yangzhou University, Yangzhou 225000, China.

Received: 19 January 2024 Accepted: 25 February 2024
Published online: 11 March 2024

References

1. Ciriminna R, Fidalgo A, Scurria A, Ilharco LM, Pagliaro M. Pectin: new science and forthcoming applications of the most valued hydrocolloid. Food Hydrocoll. 2022;127:107483. https://doi.org/10.1016/j.foodhyd.2022.107483.
2. Wang L, He F, Huang Y, He J, Yang S, Zeng J, et al. Genome of wild mandarin and domestication history of mandarin. Mol Plant. 2018;11(8):1024–37. https://doi.org/10.1016/j.molp.2018.06.001.

3. Liang PL, Chen XL, Gong MJ, Xu Y, Tu HS, Zhang L, et al. Guang Chen Pi (the pericarp of Citrus reticulata Blanco's cultivars 'Chachi') inhibits macrophage-derived foam cell formation. J Ethnopharmacol. 2022;293:115328. https://doi.org/10.1016/j.jep.2022.115328.
4. Yu X, Sun S, Guo Y, Liu Y, Yang D, Li G, et al. Citri reticulatae pericarpium (Chenpi): botany, ethnopharmacology, phytochemistry, and pharmacology of a frequently used traditional Chinese medicine. J Ethnopharmacol. 2018;220:265–82. https://doi.org/10.1016/j.jep.2018.03.031.
5. Platt D, Raz A. Modulation of the lung colonization of B16–F1 melanoma cells by citrus pectin. J Natl Cancer Inst. 1992;84(6):438–42. https://doi.org/10.1093/jnci/84.6.438.
6. Singh B, Singh JP, Kaur A, Singh N. Phenolic composition, antioxidant potential and health benefits of citrus peel. Food Res Int. 2020;132:109114. https://doi.org/10.1016/j.foodres.2020.109114.
7. Hwang SL, Shih PH, Yen GC. Neuroprotective effects of citrus flavonoids. J Agric Food Chem. 2012;60(4):877–85. https://doi.org/10.1021/jf204452y.
8. Yin Q, Chen J, Ma S, Dong C, Zhang Y, Hou X, et al. Pharmacological inhibition of galectin-3 ameliorates diabetes-associated cognitive impairment, oxidative stress and neuroinflammation in vivo and in vitro. J Inflamm Res. 2020;13:533–42. https://doi.org/10.2147/JIR.S273858.
9. Wang Y, Zhang X, Zhou C, Khan H, Fu M, Cheang WS. Citri reticulatae pericarpium (Chenpi) protects against endothelial dysfunction and vascular inflammation in diabetic rats. Nutrients. 2022. https://doi.org/10.3390/nu14245221.
10. Srimathi R, Gurunathan J. Metabolites from the citrus extracts inhibit the activity of selected proteins in Indian Cobra (Naja naja) venom. J Ethnopharmacol. 2020;252:112575. https://doi.org/10.1016/j.jep.2020.112575.
11. Yang J, Wen L, Zhao Y, Jiang Y, Tian M, Liu H, et al. Structure identification of an arabinogalacturonan in Citrus reticulata Blanco 'Chachiensis' peel. Food Hydrocoll. 2018;84:481–8. https://doi.org/10.1016/j.foodhyd.2018.06.022.
12. Peng Z, Tian S, Li H, Zhu L, Zhao Z, Zheng G, et al. Extraction, characterization, and antioxidant properties of cell wall polysaccharides from the pericarp of Citrus reticulata cv. Chachiensis. Food Hydrocoll. 2023;136:108237. https://doi.org/10.1016/j.foodhyd.2022.108237.
13. Cui J, Zhao C, Feng L, Han Y, Du H, Xiao H, et al. Pectins from fruits: Relationships between extraction methods, structural characteristics, and functional properties. Trends Food Sci Technol. 2021;110:39–54. https://doi.org/10.1016/j.tifs.2021.01.077.
14. Ohta Y, Lee JB, Hayashi K, Fujita A, Park DK, Hayashi T. In vivo anti-influenza virus activity of an immunomodulatory acidic polysaccharide isolated from Cordyceps militaris grown on germinated soybeans. J Agric Food Chem. 2007;55(25):10194–9. https://doi.org/10.1021/jf0721287.
15. Grønhaug TE, Kiyohara H, Sveaass A, Diallo D, Yamada H, Paulsen BS. Beta-d-(1→4)-galactan-containing side chains in RG-I regions of pectic polysaccharides from Biophytum petersianum Klotzsch. Contribute to expression of immunomodulating activity against intestinal Peyer's patch cells and macrophages. Phytochemistry. 2011;72(17):2139–47. https://doi.org/10.1016/j.phytochem.2011.08.011.
16. Zhang X, Bi C, Shi H, Li X. Structural studies of a mannoglucan from Cremastra appendiculata (Orchidaceae) by chemical and enzymatic methods. Carbohydr Polym. 2021;272:118524. https://doi.org/10.1016/j.carbpol.2021.118524.
17. van den Hoogen BM, van Weeren PR, Lopes-Cardozo M, van Golde LM, Barneveld A, van de Lest CH. A microtiter plate assay for the determination of uronic acids. Anal Biochem. 1998;257(2):107–11. https://doi.org/10.1006/abio.1997.2538.
18. Pettolino FA, Walsh C, Fincher GB, Bacic A. Determining the polysaccharide composition of plant cell walls. Nat Protoc. 2012;7(9):1590–607. https://doi.org/10.1038/nprot.2012.081.
19. Needs PW, Selvendran RR. Avoiding oxidative degradation during sodium hydroxide/methyl iodide-mediated carbohydrate methylation in dimethyl sulfoxide. Carbohydrate Res. 1993;245(1):1.
20. Rozi P, Abuduwaili A, Ma S, Bao X, Xu H, Zhu J, et al. Isolations, characterizations and bioactivities of polysaccharides from the seeds of three species Glycyrrhiza. Int J Biol Macromol. 2020;145:364–71. https://doi.org/10.1016/j.ijbiomac.2019.12.107.
21. Yang B, Zhao M, Prasad KN, Jiang G, Jiang Y. Effect of methylation on the structure and radical scavenging activity of polysaccharides from longan (Dimocarpus longan Lour.) fruit pericarp. Food Chem. 2010;118(2):364–8. https://doi.org/10.1016/j.foodchem.2009.04.128.
22. Chai Y, Kan L, Zhao M. Enzymatic extraction optimization, anti-HBV and antioxidant activities of polysaccharides from Viscum coloratum (Kom.) Nakai. Int J Biol Macromol. 2019;134:588–94. https://doi.org/10.1016/j.ijbiomac.2019.04.173.
23. Wang J, Shi S, Li F, Du X, Kong B, Wang H, et al. Physicochemical properties and antioxidant activity of polysaccharides obtained from sea cucumber gonads via ultrasound-assisted enzymatic techniques. LWT. 2022;160:113307. https://doi.org/10.1016/j.lwt.2022.113307.
24. Cano A, Acosta M, Arnao MB. A method to measure antioxidant activity in organic media: application to lipophilic vitamins. Redox Rep. 2000;5(6):365–70. https://doi.org/10.1179/135100000101535933.
25. Li C, Zhang Y, Zhao C, Fu X. Physicochemical characterization, antioxidative and immunoregulatory activity of polysaccharides from the flower of Hylocereus undatus (Haw.) Britton et Rose. Int J Biol Macromol. 2023;251:126408. https://doi.org/10.1016/j.ijbiomac.2023.126408.
26. Zhang X, Cai Z, Mao H, Hu P, Li X. Isolation and structure elucidation of polysaccharides from fruiting bodies of mushroom Coriolus versicolor and evaluation of their immunomodulatory effects. Int J Biol Macromol. 2021;166:1387–95. https://doi.org/10.1016/j.ijbiomac.2020.11.018.
27. do Nascimento Santos DKD, da Silva Barros BR, de Souza Aguiar LM, da Cruz Filho IJ, de Lorena VMB, de Melo CML, et al. Immunostimulatory and antioxidant activities of a lignin isolated from Conocarpus erectus leaves. Int J Biol Macromol. 2020;150:169–77. https://doi.org/10.1016/j.ijbiomac.2020.02.052.
28. Kumar A, Sharma C. Recent update of the various sources originating ghost peaks in gas chromatography: a review. J Chromatogr A. 2022;1685:463625. https://doi.org/10.1016/j.chroma.2022.463625.
29. Bermudez-Oria A, Fernandez-Prior A, Luisa Castejon M, Rodriguez-Gutierrez G, Fernandez-Bolanos J. Extraction of polyphenols associated with pectin from olive waste (alperujo) with choline chloride. Food Chem. 2023;419:136073. https://doi.org/10.1016/j.foodchem.2023.136073.
30. Carpita NC, Shea EM. Linkage structure of carbohydrates by gas chromatography-mass spectrometry (GC–MS) of partially methylated alditol acetates. In: Biermann CJ, McGinnis GD, editors. Analysis of carbohydrates by GLC and MS. Boca Raton: CRC Press; 2021. p. 157–216.
31. Ferreira SS, Passos CP, Madureira P, Vilanova M, Coimbra MA. Structure–function relationships of immunostimulatory polysaccharides: a review. Carbohydr Polym. 2015;132:378–96. https://doi.org/10.1016/j.carbpol.2015.05.079.
32. Cipriani TR, Mellinger CG, Gorin PA, Iacomini M. An arabinogalactan isolated from the medicinal plant Maytenus ilicifolia. J Nat Prod. 2004;67(4):703–6. https://doi.org/10.1021/np034043f.
33. Cui SW, Phillips GO, Blackwell B, Nikiforuk J. Characterisation and properties of Acacia senegal (L.) Willd. Var. senegal with enhanced properties (Acacia (sen) SUPERGUM™): Part 4. Spectroscopic characterisation of Acacia senegal var. senegal and Acacia (sen) SUPERGUM™ arabic. Food Hydrocoll. 2007;21(3):347–52. https://doi.org/10.1016/j.foodhyd.2006.05.009.
34. Nie S-P, Wang C, Cui SW, Wang Q, Xie M-Y, Phillips GO. The core carbohydrate structure of Acacia seyal var. seyal (Gum arabic). Food Hydrocoll. 2013;32(2):221–7. https://doi.org/10.1016/j.foodhyd.2012.12.027.
35. Odonmazig P, Ebringerova A, Machova E, Alfoldi J. Structural and molecular properties of the arabinogalactan isolated from Mongolian larchwood (Larix dahurica L.). Carbohydr Res. 1994;252:317–24. https://doi.org/10.1016/0008-6215(94)90028-0.
36. Ghosh K, Takahashi D, Kotake T. Plant type II arabinogalactan: Structural features and modification to increase functionality. Carbohydr Res. 2023;529:108828. https://doi.org/10.1016/j.carres.2023.108828.
37. Rakhmanberdyeva RK, Zhauynbayeva KS, Senchenkova SN, Shashkov AS, Bobakulov KM. Structure of arabinogalactan and pectin from the Silybum marianum. Carbohydr Res. 2019;485:107797. https://doi.org/10.1016/j.carres.2019.107797.
38. Wang L, Zhao Z, Zhao H, Liu M, Lin C, Li L, et al. Pectin polysaccharide from Flos Magnoliae (Xin Yi, Magnolia biondii Pamp. flower buds): hot-compressed water extraction, purification and partial structural characterization. Food Hydrocoll. 2022;122:107061. https://doi.org/10.1016/j.foodhyd.2021.107061.
39. Makarova EN, Shakhmatov EG. Structural characteristics of oxalate-soluble polysaccharides from Norway spruce (Picea abies) foliage. Carbohydr Polym. 2020;246:116544. https://doi.org/10.1016/j.carbpol.2020.116544.

40. Golovchenko VV, Khlopin VA, Patova OA, Feltsinger LS, Bilan MI, Dmitrenok AS, et al. Pectin from leaves of birch (Betula pendula Roth.): results of NMR experiments and hypothesis of the RG-I structure. Carbohydr Polym. 2022;284:119186. https://doi.org/10.1016/j.carbpol.2022.119186.
41. Fransen CT, Haseley SR, Huisman MM, Schols HA, Voragen AG, Kamerling JP, et al. Studies on the structure of a lithium-treated soybean pectin: characteristics of the fragments and determination of the carbohydrate substituents of galacturonic acid. Carbohydr Res. 2000;328(4):539–47. https://doi.org/10.1016/s0008-6215(00)00130-0.
42. Ponder GR, Richards GN. Arabinogalactan from western larch, Part II; a reversible order-disorder transition. J Carbohydr Chem. 1997;16(2):195–211. https://doi.org/10.1080/07328309708006521.
43. Pak U, Yu Y, Ning X, Ho C, Ji L, Mayo KH, et al. Comparative study of water-soluble polysaccharides isolated from leaves and roots of Isatis indigotica Fort. Int J Biol Macromol. 2022;206:642–52. https://doi.org/10.1016/j.ijbiomac.2022.02.187.
44. Leivas CL, Iacomini M, Cordeiro LM. Pectic type II arabinogalactans from starfruit (Averrhoa carambola L.). Food Chem. 2016;199:252–7. https://doi.org/10.1016/j.foodchem.2015.12.020.
45. Ji X, Cheng Y, Tian J, Zhang S, Jing Y, Shi M. Structural characterization of polysaccharide from jujube (Ziziphus jujuba Mill.) fruit. Chem Biol Technol Agric. 2021;8(1):54. https://doi.org/10.1186/s40538-021-00255-2.
46. Petersen BO, Meier S, Duus JO, Clausen MH. Structural characterization of homogalacturonan by NMR spectroscopy-assignment of reference compounds. Carbohydr Res. 2008;343(16):2830–3. https://doi.org/10.1016/j.carres.2008.08.016.
47. Vriesmann LC, de Oliveira Petkowicz CL. Polysaccharides from the pulp of cupuassu (Theobroma grandiflorum): structural characterization of a pectic fraction. Carbohydr Polymers. 2009;77(1):72–9. https://doi.org/10.1016/j.carbpol.2008.12.007.
48. Westereng B, Michaelsen TE, Samuelsen AB, Knutsen SH. Effects of extraction conditions on the chemical structure and biological activity of white cabbage pectin. Carbohydr Polymers. 2008;72(1):32–42. https://doi.org/10.1016/j.carbpol.2007.07.017.
49. Mukhiddinov ZK, Khalikov DK, Abdusamiev FT, Avloev CC. Isolation and structural characterization of a pectin homo and ramnogalacturonan. Talanta. 2000;53(1):171–6. https://doi.org/10.1016/s0039-9140(00)00456-2.
50. Yang B, Luo Y, Sang Y, Kan J. Isolation, purification, structural characterization, and hypoglycemic activity assessment of polysaccharides from Hovenia dulcis (Guai Zao). Int J Biol Macromol. 2022;208:1106–15. https://doi.org/10.1016/j.ijbiomac.2022.03.211.
51. Cui J, Zhang L, Wang J, Zhao S, Zhao C, Liu D, et al. Study on the relationship between primary structure/spatial conformation and gel properties of pectins from different varieties. Food Hydrocoll. 2023;144:109055. https://doi.org/10.1016/j.foodhyd.2023.109055.
52. Hosseini-Parvar SH, Matia-Merino L, Goh KKT, Razavi SMA, Mortazavi SA. Steady shear flow behavior of gum extracted from Ocimum basilicum L. seed: effect of concentration and temperature. J Food Eng. 2010;101(3):236–43. https://doi.org/10.1016/j.jfoodeng.2010.06.025.
53. Yoshida S, Hoppe AD, Araki N, Swanson JA. Sequential signaling in plasma-membrane domains during macropinosome formation in macrophages. J Cell Sci. 2009;122(Pt 18):3250–61. https://doi.org/10.1242/jcs.053207.
54. Porrini C, Ramarao N, Tran S-L. Dr. NO and Mr. Toxic—the versatile role of nitric oxide. Biol Chem. 2020;401(5):547–72. https://doi.org/10.1515/hsz-2019-0368.

Publisher's Note